Antisana volcano: A representative andesitic volcano of the eastern cordillera of Ecuador: Petrography, chemistry, tephra and glacial stratigraphy

Minard L. Hall [a],[*], Patricia A. Mothes [a], Pablo Samaniego [b], Annemarie Militzer [d], Bernardo Beate [c], Patricio Ramón [a], Claude Robin [b]

[a] Instituto Geofísico, Escuela Politécnica Nacional, Casilla 1701-2759, Quito, Ecuador
[b] Laboratoire Magmas et Volcans, Université Blaise Pascal - CNRS - IRD, Campus Universitaire des Cézeaux, 6 Avenue Blaise Pascal, 63178, Aubière, France
[c] Dept. Geología, Escuela Politécnica Nacional, Casilla 1701-2759, Quito, Ecuador
[d] Institute for Geosciences, Johannes Gutenberg Universität Mainz, Germany

ARTICLE INFO

ABSTRACT

Antisana volcano is representative of many active andesitic strato-volcanoes of Pleistocene age in Ecuador's Eastern Cordillera. This study represents the first modern geological and volcanological investigation of Antisana since the late 1890's; it also summarizes the present geochemical understanding of its genesis. The volcano's development includes the formation and destruction of two older edifices (Antisana I and II) during some 400 + ka. Antisana II suffered a sector collapse about 15,000 years ago which was followed by the birth and growth of Antisana III. During its short life Antisana III has generated ≥50 eruptions of small to medium intensity, often associated with andesitic to dacitic lava flows and tephra, as well as with late Pleistocene and Holocene glacial advances. Throughout its long history Antisana's lavas have been characterized by a persistent mineral assemblage, consisting of 30 −40 vol% phenocrysts of plagioclase, both clino- and orthopyroxene, and Fe-Ti oxides, with rare occurrences of olivine or amphibole, frequently in a microcrystalline to glassy matrix. This uniformity occurs despite the magma's progressive chemical evolution over ≥400 ka from early basic andesites (53−58 wt % SiO_2) to intermediate and Si-rich andesites (58−62% SiO_2), and recently to dacites (63−67% SiO_2). Chemical diagrams suggest that crystal fractionation was the most likely magmatic process of evolution. The exception to this slowly evolving history was the short-lived emission at ~210 ka of the Cuyuja lavas from Antisana II that generated a 73 km long andesitic lava flow. Contrasting with Antisana's general magmatic trend, Cuyuja lava (~11 km³) is a high-Mg andesite with unusually high concentrations of incompatible elements. Antisana developed within the Chacana caldera complex, a large active siliceous center that began ~3 Ma ago, however its lavas are chemically distinct from coeval lavas of Chacana.

© 2016 Elsevier Ltd. All rights reserved.

1. Introduction

Antisana Volcano is a large glacier-clad strato-cone in Ecuador's Eastern Cordillera, 50 km SE of Quito, Ecuador's capitol city. Along with Cayambe, Cotopaxi, Tungurahua, and Sangay volcanoes, Antisana is one of the most important strato-volcanoes that comprise the andesitic volcanic row of this cordillera (Fig. 1a and b) (Hall et al., 2008). The Ecuadorian volcanic arc consists of two parallel mountain ranges, the Western and Eastern Cordilleras that are separated by an intervening large structural depression known as the InterAndean Valley. The volcanoes of the Western Cordillera represent the arc's volcanic front whose eruptive centers are spaced systematically 30−35 km apart. Their Late Pleistocene to present activity has been silicic andesitic to dacitic in composition. The volcanic centers of the Eastern Cordillera are large 15-20 km-wide andesitic strato-volcanoes that are randomly distributed along and across the breadth of that cordillera. These centers have been slightly more active during the Late Pleistocene and Holocene than those of the Western Cordillera, Sangay volcano being the most active (Monzier et al., 1999). Their youngest eruptive products are silicic andesites of normal calc-alkaline affinity (56−63% SiO).
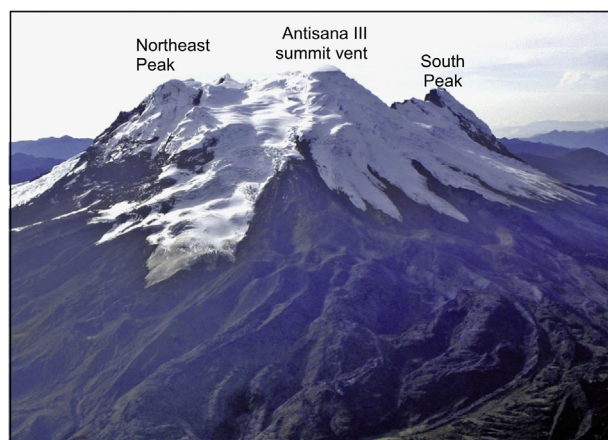
a
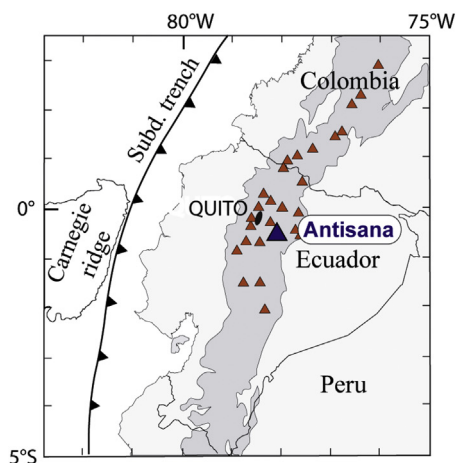
b

Fig. 1. a & b: a) Antisana volcano as seen from the northwest. Its summit (5753 m) and crater are covered by a flat glacier. The South Peak, remnant of Antisana I, is to its right. Numerous late Pleistocene and Holocene lava flows cover the northwest foot of the active cone (foreground). (photo: P. Ramón, IGEPN, 2005). b) Map of the volcanoes of Ecuador with Antisana shown in the Eastern Cordillera. The subduction trench of the Pacific Ocean's Nazca Plate is also shown.

During the past 20 years numerous young rhyolitic centers have also been identified along the Eastern Cordillera (Mothes and Hall, 2008). In some volcanoes, such as Cotopaxi, rhyolitic outbursts have been interspersed with normal andesitic activity (Hall and Mothes, 2008a; Garrison et al., 2011). Despite its location within the rhyolitic Chacana caldera and the recent bi-modal activity of nearby Cotopaxi volcano, Antisana has displayed a monotonous trend of andesitic activity during the Pleistocene, followed by a very late transition to dacitic products in the Holocene. This contribution represents the first major description of Antisana volcano, its volcanic history and chemical evolution, considered to be an excellent representative of andesitic magmatism of the Northern Andean Arc.

Antisana has built its large cone in the SE corner of the Chacana caldera complex (Fig. 2a), a large andesite and rhyolite center whose outer flanks are comprised of ignimbrites, welded tuffs, breccias, and lava flows that form a semi-circle around the 35 km-long caldera-like depression (Hall and Mothes, 2008b). Paleozoic and Mesozoic metamorphic belts comprise the underlying basement. Antisana straddles the NNE-SSW-oriented boundary that separates the metamorphic belts to the E from Quaternary volcanic rocks to the W. Antisana along with neighboring Cayambe and Cotopaxi volcanoes sits upon the Northern Andean Block (Trenkamp et al., 2002), a small tectonic sliver that is migrating to the NE (Nocquet et al., 2014).

From Antisana's snow and ice-covered summit (5753 m elevation), drainages to the N, E, and S form the Quijos River, a tributary of the large Coca River. Drainages to the W and SW form the Antisana River, a tributary of the larger Napo River. Both these large rivers are part of the Amazon River system. The volcano's edifice measures ~15 km in diameter and is slightly elongate in an E-W direction. Its steep (25-35°) outer flanks descend to the surrounding glaciated valleys at ~3200 m elevation. However, to the W and SW a broad detrital apron descends from 4400 m to 3900 m, and forms the volcano's base. Glaciers, ice falls, and ice-covered rock faces characterize most flanks down to 4700−5100 m. During the 1960's glaciers covered ~26 km^2 and had an estimated volume of 0.8 km^3, but during the past decades the ice limit has retreated upslope many hundreds of meters (Hastenrath, 1981; Cáceres et al., 2004), leaving a skirt of glacial debris around the cone's base. The surface waters from this volcanic edifice comprise one of Quito's principal water sources and it would be jeopardized by future volcanic activity.

From fissures located ~15 km to the NW and N of Antisana effusive eruptions occurred in AD 1760 and 1773, however these have more chemical similarities to lavas from Chacana than to Antisana (see below). Humboldt's 1802 sighting of smoke near Antisana remains unexplained. No Antisana ashes are found in stratigraphic sections younger than 800 aBP (this study; Ledru et al., 2013).

Reconnaissance and petrographic studies around Antisana were carried out by Humboldt (1837-38); Wolf (1892), Whymper (1987), Reiss and Stübel (1902), and Meyer (1907). Additional overviews were published by Sauer (1965), Hall (1977), Hall and Beate (1991) and Egred (2010). Volcanic hazard evaluations including a 1:50,000 scale hazards map were presented in Hall et al. (1989). The present study summarizes work that began in 1996 with a 9 day-traverse around the volcano and continued with the subsequent detailed petrographic and stratigraphic work and radiocarbon dating presented here.

2. Overall structure and morphology

Antisana's volcanic edifice is comprised of three prominent ridges of steep rock and ice that radiate from the young summit cone (Figs. 3−5). To the NE of the cone and forming the northern wall of a large glacier-filled valley is a short ENE-trending ridge that joins the summit cone to the Northeast Peak (~5650 m). This ridge is comprised of lavas and breccias whose layering dips steeply to the N and is thought to be a remnant of the northern flank of the older Antisana II edifice. From the summit cone a second short ridge arcs to the SW to form the South Peak (~5600 m), whose west side drops sub-vertically to the western base of the Antisana edifice. Its east side descends steeply into a cirque-like depression, herein referred to as the south glacial cirque. A third knife-edge ridge, bounded by near-vertical rock cliffs, runs 1.5 km eastwards from the summit cone; its high point is here called the Central Peak (5670 m). This ridge separates the large glacial valley to its N from the edifice's south face, which is comprised of lavas and breccias that are steeply inclined to the S. This third ridge continues eastwards for another kilometer before descending to its next high point, here called the Southeast Peak (4565 m); it is comprised of bedded breccias and lavas that dip to the SE.

The large glacial valley that heads on Antisana's summit descends to the E between the ridges of the Northeast and Central Peaks of the old edifice. The valley is ~1.1 km wide, ~2.3 km long, and up to 400 m deep (Fig. 3). Because of its imposing size and central location, the valley's origin by sector collapse seems likely,
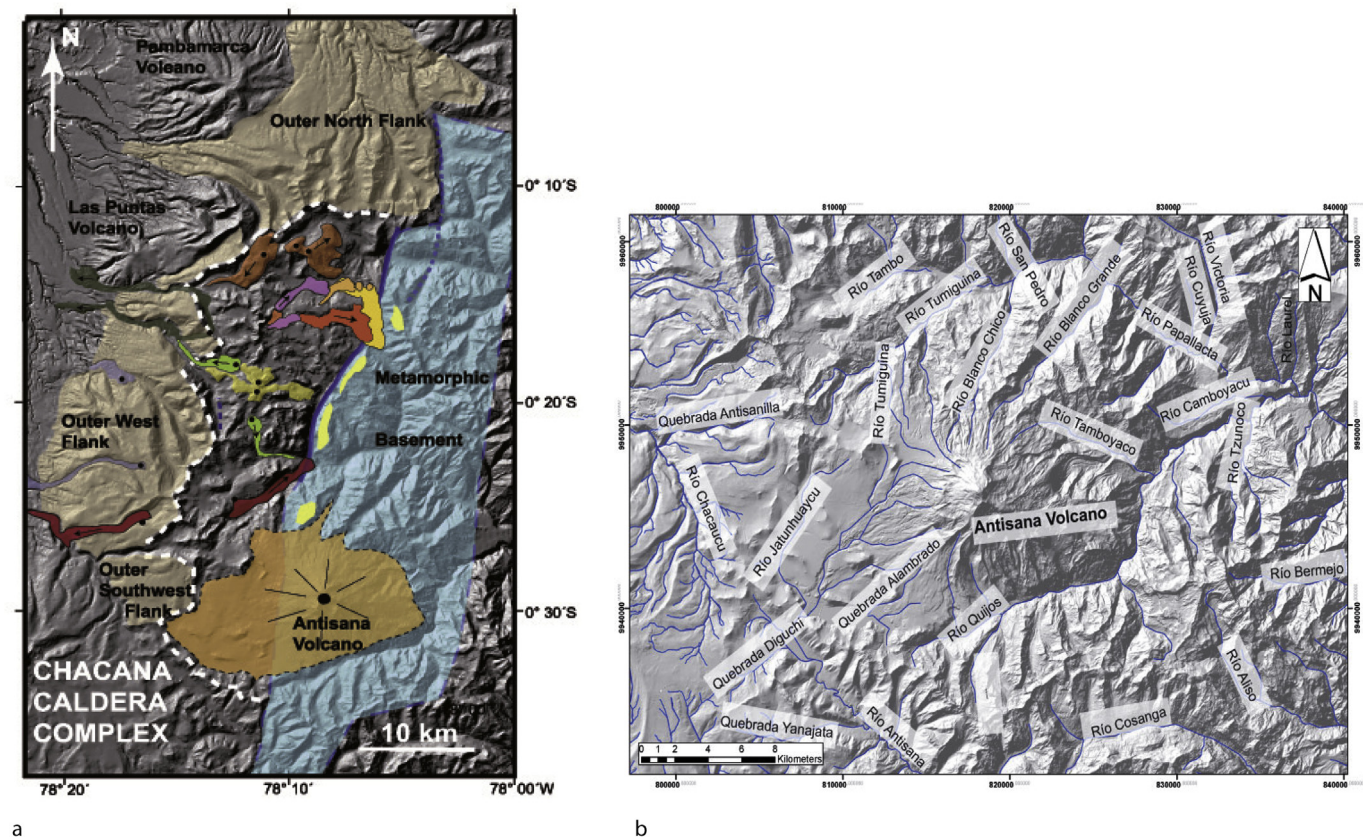
Fig. 2. a & b: a) Location of Antisana volcano within the Chacana caldera complex, showing the caldera limits (white dashed line), its outward-dipping flanks, and the Mesozoic metamorphic basement and boundary (blue). Late Pleistocene lava flows and vents shown in complex. b) Physiographic view of Antisana volcano and its drainage pattern. (For interpretation of the references to colour in this figure legend, the reader is referred to the web version of this article.)
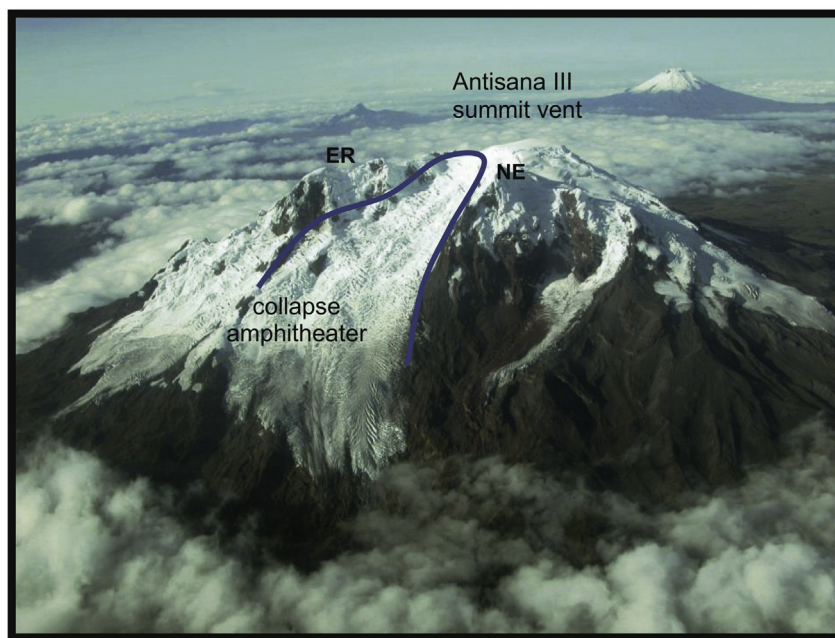
Fig. 3. In this view from the northeast, Antisana III's summit lies at the head of an amphitheater, shown by a line, thought to be of sector collapse origin. The amphitheater is bounded by the east ridge (ER) and the Northeast Peak (NE), both being remnants of the opposing flanks of the original Antisana II edifice. (photo: P. Ramón, IGEPN, 2002).

however a rock slide or a glacial origin cannot be discarded. The lava successions that make up these two ridges dip away in opposite directions, suggesting that the original vent was high above the center of this valley, just E of the present summit cone.
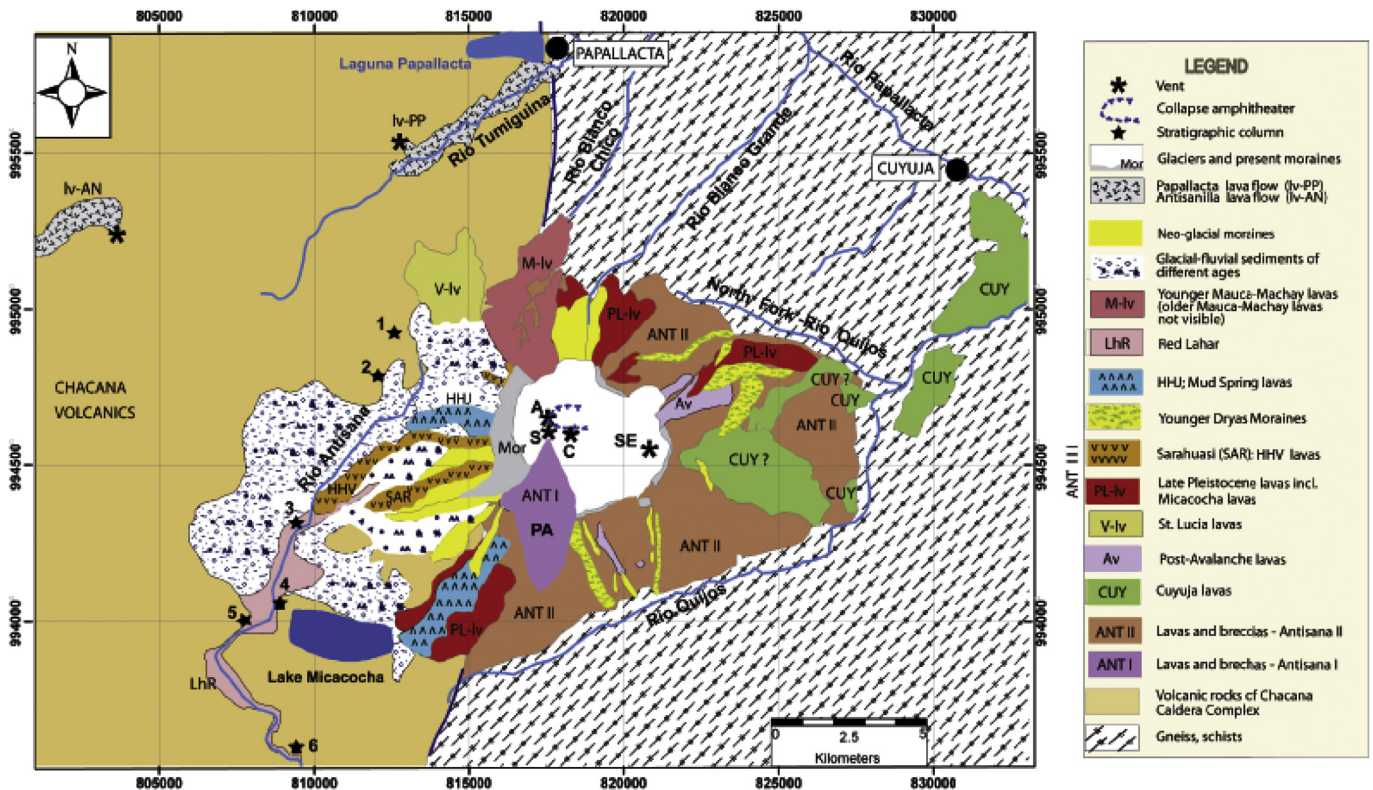
Fig. 4. Geologic sketch map of Antisana volcano and surrounding areas. See legend and text for description of units. Letters refer to: A = Antisana III crater; S= South Peak (Antisana I vent); C= Central Peak; SE= Southeast Peak; PA=Piedra Azufre site. Numbers refer to sites of stratigraphic columns: 1 = Sta. Lucia; 2 = Quebradilla; 3 = Hacienda Antisana; 4 = Micacocha gate; 5 = EMAAP water intake; 6 = Rio Antisana. CUY=Cuyuja lava outcrops-verified; CUY? = unverified. Points * lv-AN and * lv-PP refer to Chacana historic lava flows. Coordinates shown as UTM Projection South America 1956.
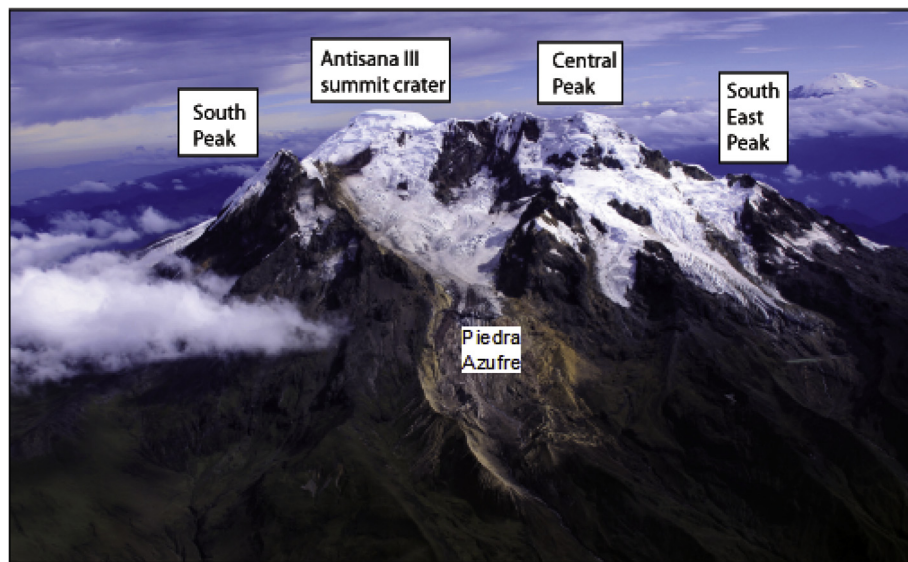
Fig. 5. View of the south flank of the Antisana edifice with South Peak (Antisana I) at far left and Antisana III's flat summit and glacier-filled crater behind. Note the glacial cirque in front of the west-east ridge with its Central Peak and to its right the Southeast Peak, both of Antisana II. The hydrothermally-altered core of Antisana I is being eroded by glaciers, leaving yellow till deposits. (photo: P. Ramón-IGEPN, 2010).

3. Antisana I

Three distinct eruptive centers or edifices are recognized on Antisana. The early Antisana I edifice is centered upon or near South Peak (Figs. 4 and 5), whose structure is that of a steep-sided cone comprised of lava and breccia sequences that are inclined steeply (~35°) away to the SW. Near South Peak's summit, tephra beds fill a bowl-shaped structure, ~300 m across, presumed to be remnants of Antisana I's extinct crater. Immediately E of South Peak exists a cirque-like depression, open to the S and less than 1 km in

diameter, where a ≥400 m-thick series of interbedded lavas and breccias are observed (symbol PA in Fig. 4) that dip moderately to the S and SW; the thick series suggests that Antisana I had a long history. Antisana I's interior is extensively altered hydrothermally (Fig. 5). The eastern wall of the cirque is part of the Antisana II edifice and shows no signs of alteration, implying that Antisana I is the older edifice. In conclusion the Antisana I edifice had a small volume (~5.4 km^3) and represents the older Antisana edifice.

4. Antisana II

The Antisana II edifice is centered on the Central Peak or slightly northward. All the N, E and S outer flanks of the present Antisana massif appear to be remnant flanks of Antisana II, as their lava sequences dip away from Central Peak ridge (Figs. 4–6). The Southeast Peak was a likely satellite vent of Antisana II, as late lavas apparently descended from it.

4.1. Principal lava sequences

On the upper S side of Antisana II's large massif, lava flows and breccia units dip steeply southward and are largely covered by glaciers and snowfields. At the base of its steep cliffs a sequence of stacked lava flows and interbedded breccias continues down slope for many more hundreds of meters, of which only a few have been sampled and analyzed. This sequence continues around the E side of the edifice (Figs. 5 and 6), where it extends out from under the ice and snow cover and forms cliffs up to 100 m high. Their thicknesses, inclined orientation, and lower elevation would suggest that these sequences belong to an early stage of Antisana II's edifice construction.

Antisana's NE flank, dominated by the Northeast Peak, is made up of steep northward-dipping sequences of inter-bedded breccias, tephra, and 6-10 m-thick lavas units. Its lower flanks are also comprised of a thick series of older lava flows, petrographically similar to those observed on the E side. Many are traceable

northwards down slope until they end upon the metamorphic basement. The flows are generally 100–200 m wide, 5–20 m thick, and up to 4 km long. Their compositions (57–60 wt% SiO$_2$) differ little from lavas of Antisana II's east and south flanks (Figs. 6 and 7). The lavas are frequently inter-bedded with breccia units that carry fragments of Antisana II lavas. Late Pleistocene dacitic lavas often override these older lavas in the NNW to NNE quadrant.

4.2. Younger lavas of the Southeast Peak of Antisana II

On the SE flank of the old Antisana II edifice and overlying the above-described sequences extends a large, slightly-inclined surface formed by another series of lava flows and inter-bedded breccias. At least 12 individual lava flows comprise the top of this series, each about 8–20 m thick, accompanied by breccias that range from 5 to 8 m in thickness. This series of SE-dipping lava sheets has its apex on or near the Southeast Peak, its probable source vent. These lavas post-date the south flank succession of Antisana II, as they fill an eroded valley cut into the south flank lavas. They are petrographically similar to most Antisana II lavas.

4.3. The Cuyuja lavas

Perhaps the most interesting event in Antisana's history corresponds to the appearance of unusually long, chemically unique, andesitic lava flows, herein called the Cuyuja lava flows. They are traceable from the SE foot of Antisana II's edifice down the Quijos River valley for 73 km (Fig. 7). Along this trajectory the flows have left numerous flat lava terraces, which today are the sites of Cuyuja, Baeza, Borja, Chaco, and Santa Rosa towns, as well as that of extensive flat agricultural land. The Cuyuja lavas are dark gray to black porphyritic andesites with phenocrysts of plag (15–25 vol%), ol (5–8%), cpx (≤5%), opx (≤1%) in a microcrystalline to glassy matrix (55–60%) that carries parallel-oriented microlites of plag, cpx, and Fe-Ti oxides. Seven to ten distinct lava flows are recognized, apparently coeval in time, as only a trace of river sediment is

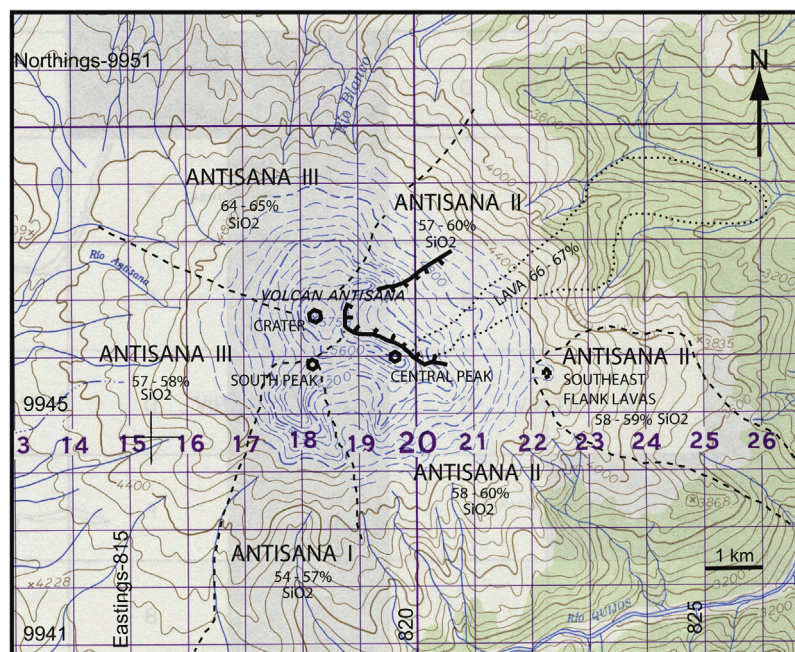**Fig. 6.** Map of the approximate petrologic groupings of lavas according to their SiO$_2$ contents. The location of Antisana III's crater and the limits of its collapse amphitheater (hachured line) are also indicated. Map shown as Universal Transverse Mercator (UTM) (Projection South America, 1956). Northings UTM 9941 to 9951; Eastings UTM 813 to 826. Digital Map Base, Volcán Antisana; Instituto Geográfico Militar, Quito.
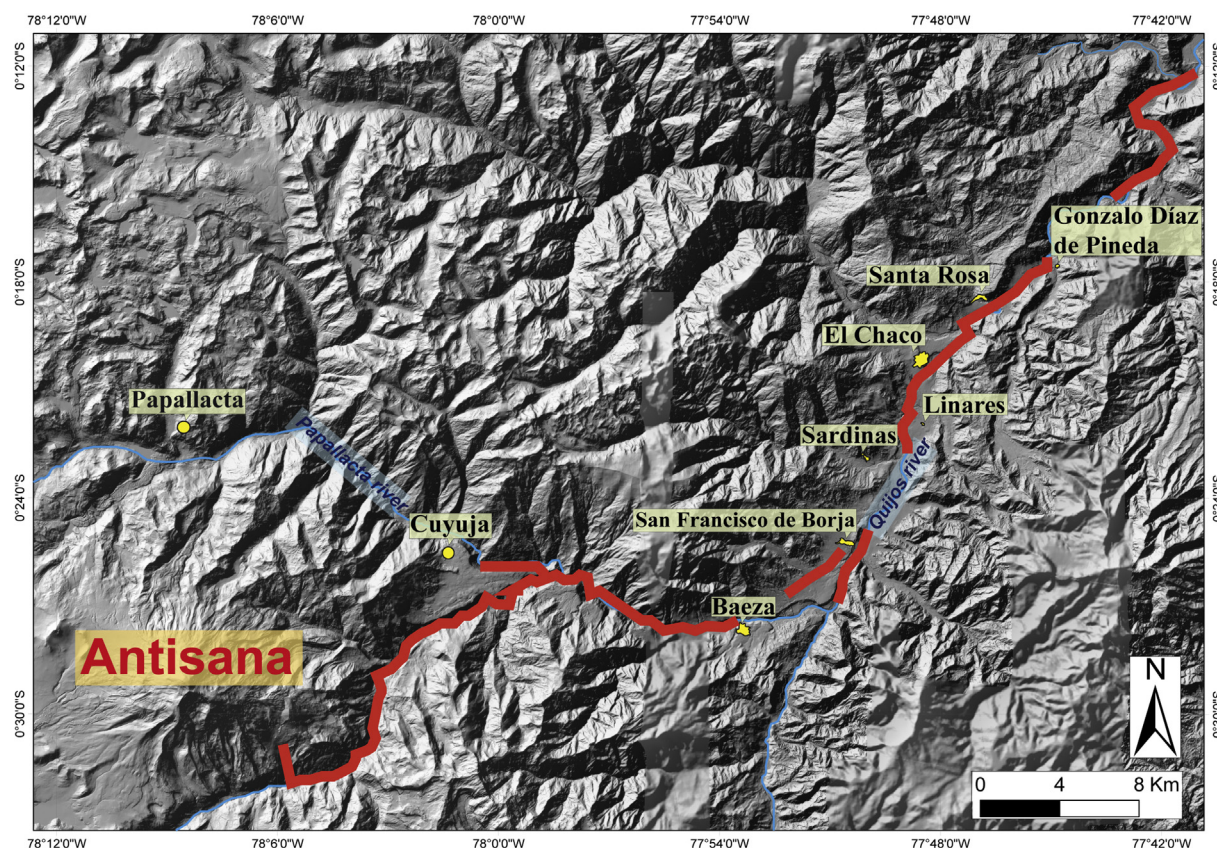
Fig. 7. DEM map showing a major portion in red of the 73 km-long Cuyuja lava flow, traceable from Antisana II's SE side down the Quijos river valley. Note the prominent lava terraces used as town sites and agricultural lands. (For interpretation of the references to colour in this figure legend, the reader is referred to the web version of this article.)

occasionally observed between the individual flow units. Many have columnar jointing, implying that short cooling periods transpired between some flows. Notably these are high Mg andesites (~56% SiO_2), chemically unlike most Antisana lavas.

An Ar-Ar date of 210 ± 30 ka was obtained for the prominent basal flow unit near Baeza (Opdyke et al., 2006).

The source of the Cuyuja lava flows lies near the SE corner of Antisana II's edifice, the site of their farthest up-river lava terraces on the Quijos River, where this lava forms a 300 m-thick terrace. Unfortunately, Cuyuja lavas were not found during sampling on Antisana's upper slopes. At 8 km downstream, where the flows spilled out of the Quijos river canyon into the adjacent valley of Cuyuja town, the combined flows are 320—340 m-thick. At 25 km downstream, they are ~280 m-thick, at 34 km—200 m-thick, at 66 km—30 m-thick, and they end at 73 km (Fig. 8). The flows have an estimated surface area and volume of 100 km^2 and 11 km^3, respectively. The great distance traveled by some flows is attributed in part to the relatively narrow (100-500 m-wide) valleys that the flows descended, valley gradients of 0.3%—0.015%, the flow's notable volume, possibly to rapid emplacement, and/or to favorable rheological properties of the lava (Keszthelyi and Self, 1998).

Where the lavas entered the adjacent Papallacta River valley near Cuyuja town, they dammed that river, resulting in a small lake, which over time developed a 74 m-thick sequence of repeated beds, each 10-20 cm-thick, of lacustrine silts and sands and occasional debris flows. The sands are chiefly comprised of reworked juvenile scoria lapilli and ash that fell into the greater Antisana drainage basin and were remobilized by streams to their final resting sites. The deposit's thickness and repetitive character suggest that Antisana's eruptive activity persisted for considerable time after the lava's emplacement.

4.4. Radiometric dates of Antisana II

Several Ar-Ar radiometric dates were provided by J-P. Eissen (IRD) (Table 1). Samples AN45 (58.4% SiO_2), sample ANT60 (58.0% SiO_2), and sample AN51 (59.5% SiO_2), all typical andesites, provide tentative ages of 378 ± 38 ka, 280 ± 33 ka, and 276 ± 22 ka, respectively. These correspond to an approximate mid-way height (4400—4600 m elevation) up Antisana II's southern flank. AN45 belongs to the main core of the edifice, while AN60 and AN51 belong to younger slopes of the main edifice.

Lavas that occur toward the SE corner of Antisana II's edifice and that share a similar chemistry (59% SiO_2) give Ar-Ar dates of 253 ± 23 ka (AN38) and 190 ± 23 ka (AN43). This youngest sample from Antisana II's edifice came from outcrops at ~4500 m elevation, about 1200 m short of the south flank's total height; this implies that Antisana II remained active for considerable time after AN43's emission. This last sample has a value similar to the 210 ± 30 ka Ar-Ar date obtained for the Cuyuja lava flow (Opdyke et al., 2006), which had filled an already deeply-dissected valley cut into Antisana II's southern flank by 210 ka, implying that early Antisana II magmatism occurred long before 210 ka. As a consequence Antisana's total age must be considerably older. We estimate that the total Antisana II edifice had a volume of ~33 km^3 and an age greater than 400 ka.

4.5. Post-avalanche lavas

Earlier, in the discussion of Antisana's morphology, a sector collapse was proposed to explain the large valley that heads on the present Antisana summit. This presumed sector collapse of ~0.5—1 km^3 volume followed Antisana II's formation, whose
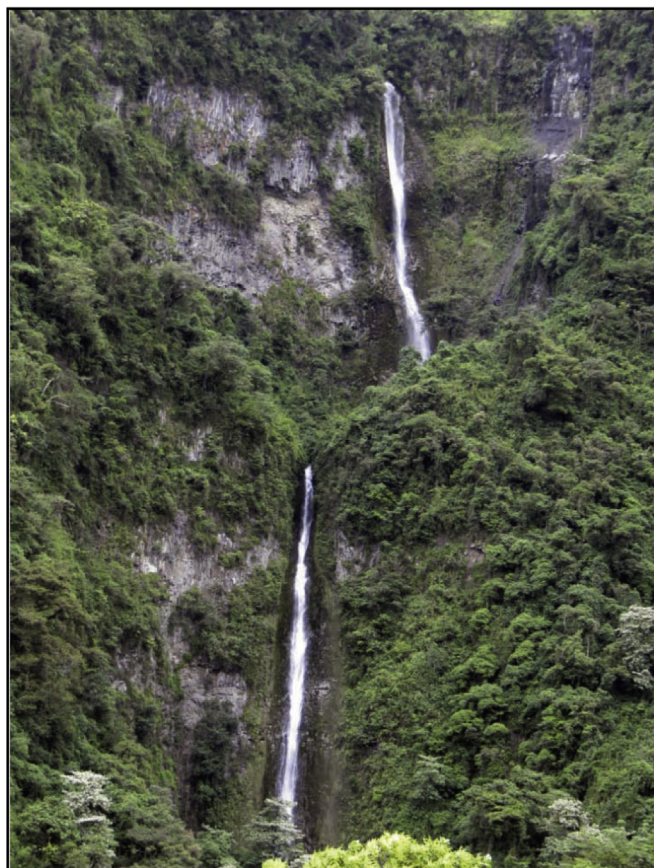
Fig. 8. The Cuyuja lava series, consisting of 6–7 distinct flows of basic andesite, strongly columnar-jointed, whose total thickness here is ~300 m. (photo: J. Rehda, 2011).

youngest lavas are less than 190 ka. Two post-collapse lava flows are traceable by their lobate morphology down the amphitheater valley to where they protrude from under the present valley glacier and rest in turn upon older Antisana II lavas. These lavas, ANT 30 and 32, are Si and K-rich dacites (67% SiO_2) that represent the most siliceous rocks found on any Antisana edifice. As such, their location and late arrival imply that they are related to a late intrusion of silicic magma that may have led to a sector collapse. Furthermore, these lavas are similar chemically to the Mauca-Machay series of Antisana III's dacitic lavas, further implying that the sector collapse and the dacitic magmatism occurred jointly in late Pleistocene times. Early in post-collapse times the magma source shifted to the Antisana III vent near the volcano's present summit.

The timing of the sector collapse is proposed by the glacial morphology. Paired Younger Dryas (YD) lateral moraines are observed in most upper Antisana valleys and their presence would suggest that a sector collapse in the amphitheater valley would have had to happen prior to the YD glaciation. Late Glacial

Maximum (LGM) glaciers would have descended this valley earlier. However, while the right lateral moraine of the LGM is clearly present in this valley, as well as at its final terminal moraine farther down valley, its left lateral moraine is not evident. One could argue that the missing left lateral LGM moraine was carried away by the descending avalanche from the sector collapse. If this happened, it would imply that the sector collapse would have occurred sometime between the LGM and the YD glaciations, roughly between ~15 and 11 ka (Clapperton et al., 1997). The youthful age of this scenario would fit in well with the conclusion that the post-collapse lavas of the amphitheater best match the youngest Antisana III Si-rich lavas, thought to be Late Pleistocene in age.

5. Antisana III

5.1. Introduction

Antisana III is the youngest vent and forms the present summit (5753 m) on the west side of the well-eroded Antisana II edifice (Figs. 1a and 6). Its summit has a flattened conical form, presumably due to glacial-infilling of its crater. All Late Pleistocene and Holocene lava flows originated at this summit and flowed mainly to the N, W, and SW. Young lava flows can be traced up slope under the western and northern glaciers toward the summit, verifying that the summit cone is the present emission vent. Around the western base of the edifice, a large volcano-clastic apron has developed, comprised of thick sequences of tephra, lavas, pyroclastic flow units, debris flow deposits, and their detrital products. Based upon the regional tephra stratigraphy, Antisana III's cone formed during the Late Pleistocene and Holocene. Fumarole vents have not been identified on the edifice, however mountaineers sometimes report the odor of SO_2 gas at the higher elevations. Antisana III was the source of both andesitic and dacitic emissions at the end of the Pleistocene to mid Holocene, as both lava types can be traced to the present crater.

Antisana's recent history is best recorded in the tephra and lava stratigraphy exposed on the volcano's western slopes. The W-NW side, being proximal to and downwind from the summit crater, displays the most complete tephra sequence of Antisana III, followed by the SW side which tends to have thinner deposits. Two composite stratigraphic columns from the lower NW and SW flanks of Antisana III are given in Figs. 9 and 10, respectively, which present the tephra, glacial, and lava stratigraphy in chronological order. The most complete sequences are found in the Santa Lucia and Quebradilla ravines in the NW sector (Fig. 11). The SW composite section is based upon outcrops near the Hacienda Antisana, the Micacocha control gate, the EMAAP water intake, and downstream along the Antisana River (Fig. 4). Four successions of bedded units are recognized in each of the two columns and they are roughly inter-correlated by means of their distinguishing characteristics as well as by guide units whose ages are approximately known. Seven new radiocarbon dates are given in the text or in Figs. 9 and 10; nine others are referenced. Scarcity of datable material limited radiocarbon dating of more eruptive events.

Table 1
Ar–Ar age dates of several lavas from Antisana II.

Sample	Approximate Location on Antisana II	Precise Location as UTM PSA 56	Ar-Ar age (ka)	Source
AN-45	S face	82015-994418 4610 m	378 ± 38	J-P. Eissen (IRD)
AN-60	SW corner	81713-99429 4460 m	280 ± 3	J-P. Eissen (IRD)
AN-51	S corner	82035-994369 4380 m	276 ± 22	J-P. Eissen (IRD)
AN 38	SE corner	82216-994582 4520 m	253 ± 23	J-P. Eissen (IRD)
AN 43	SE flank	82132-994420 4510 m	190 ± 23	J-P. Eissen (IRD)
Cuyuja Lava	Baeza	17494-994922 1880 m	210 ± 30	Opdyke et al., 2006

Composite Column for NW Sector, Antisana Volcano

Succession M Top Based upon Sections at Quebradilla and Sta. Lucia (Fig. 4)

Succession A
(~6.5 m thick)

Small to
moderate
scoria-rich
eruptions
w/ repose
periods of
1-2 ky

- .25 -Soil; silty w/ no obvious clasts. Surface has abundant cushion plants
- .20 -RW fine Quilotoa AF that grades into soil above. +++ biotite. 800 aBP **
- .45 -Soil; ashy. lithic & scoria lapilli in center. MP= 3 cm; ML= 0.5 cm
  Dark kaki scoria AF; large plag. xls. (Last eruption of Antisana) = M-M lavas **ANTI-41**
- .11 -Fine sandy yellow AF; ++amphibol. G. Pichincha AF of 1100 aBP ****
- .13 -Black lithic lapilli AF; fresh & angular. No scoria. Scarce white pumice frags. ML= 2 cm. Dome explosion? **ANTI-40**
- .22 -Grey & rosy-colored sandy ash. Few scoria clasts. PF related to M-M lava eruption? **ANTI-39**
- .44 -Dirty AF in soil; contains white pumice grains (10%), grey lithics (30%), sand (60%); =Cotopaxi "KA" AF;
  Soil dated at Cotopaxi (2050 +/- 80; 2170 +/- 100; 2310 +/- 90 aBP) *
- .15 -Black coarse lithic & xl-rich sandy AF **ANTI-38**. **(Sample HAL-61)**
- .02 -AF w/ off-white pumice, grey lithics, black glassy lithic grains **ANTI-37**
- .15 -Dark brown organic soil; w/ carbon dispersed at upper contact (Top dated 3400 +/- 150 aBP ✝). Hardpan at base.
- .06 -White fine sandy ash; = Cotopaxi F5 rhyolitic plinian AF; dated at between 5940+/- 30; 5830 +/- 80 and 4670 +/- 70 aBP * 5885 +/- 30 aBP ✝
- .45 -Dark grey to black organic soil w/ occasional pumice grains
- .05 -White rhyolitic pumice lapilli AF; MP= 0.5 cm. Urcucuy Dome lapilli AF
- .20 -Dark brown organic soil; w/ carbon dispersed at upper contact (Top dated- 6440 +/- 30✝; 6685 +/-30 aBP ✝
- .30 -Black coarse sandy scoriaceous AF- May be related to Huagra Halina Lava--7395 +/- 30 aBP ✝; 7400 +/- 30 aBP ✝ **ANTI-36**
- .05 -Medium grey-brown soil

Succession B
(not present-
see SW
section)

- .15 -White rhyolitic fine pumice lapilli AF w/ finer ash top; = Cotopaxi F2 plinian AF = 7770 +/- 70 aBP *
- 1.5 -Black medium sandy scoriaceous AF. RW at top. **ANTI-35**
- .20 -Yellow-white rhyolitic med. sandy AF. Distal source. ++ small biotite. = Huañuna II ~10,075 +/- 50 aBP ***
  -Erosional unconformity.
- .60 -Black medium sandy scoriaceous AF; laminated at base. **ANTI-34**
- 1.5 -Black coarsely-layered scoriaceous, med. sandy AF; w/ occasional angular red or grey lithic clasts,
  1-3 mm av. size **ANTI-33**
- .08 -Black clayey to fine sandy AF **ANTI-32**
- .02 -Coarse-grained, altered lithic AF **ANTI-31**

Succession C
(~8.2 m thick)

Series of
energetic
scoria-rich
eruptions
w/ short
repose
periods

- .02 -White pumice lapilli AF; MP= 3 cm. w/ altered lithics. Local source? **ANTI-30**
- .08 -Black scoriaceous med. sandy AF; laminated at base. **ANTI-29**
- .03 -Yellow med.-grained hardened pumice AF **ANTI-28**
- .23 -Black scoriaceous, coarse sandy ash & lithic AF. Layer of fine yellow-mauve ash in middle. **ANTI-27**
- .13 -Beige to yellow fine sandy AF **ANTI-26**
- .80 -Black med. grain scoriaceous AF. Massive with no obvious bedding. **ANTI-25**
- .35 -Debris flow deposit w/ tabular lava clasts. Disturbed by solufluction.
- .02 -Brown clayey lens
- .09 -Coarse sandy pumice & lithic AF; poorly sorted. MP= 0.5-1 cm **ANTI-24**
- .50 -Massive black coarse sandy AF. No obvious bedding. **ANTI-23**
- .15 -Black, well laminated, med. sandy AF; alternating fine to coarse layers. **ANTI-22**
- .16 -Coarse pumice, scoria & lithic lapilli AF; w/ indurated gray lithic ash in center, MP= 1 cm
- .02 -Dense pumice & lithic AF; MP= 2.5 cm. Some altered clasts at base. **ANTI-21**
- .15
- 1.6 -Fine laminations of black, fine-sandy AF, not RW. Homogeneous grain size.
  Clay lens in center. **ANTI-20**
- .16 -Lithic AF= 3 layers =? HHV and Sarahuasi lavas. **ANTI-19**
  -Fine silty indurated AF; phreato-magmatic AF lens?
- 1.4 -Dense, off-white, pumice lapilli AF. Fresh, un-altered. Pumice= 65 wt% SiO2.
  MP= 6 cm, ML= 2 cm. w/ hardpan at base. Dated at 13,900 +/- 440 aBP ✝ **ANTI-18 (HAL-62 & -84)**
- .25 -Black scoria & lithic lapilli AF. No sorting **ANTI-17**
- .20 -Clayey, orange-colored varves, finely laminated.
- .10 -Lithic AF **ANTI-14**
- .20 -Silty varve layers.

Succession D
(~9.3 m thick)

Waning LGM
glacial-fluvial
beds intercalated
w/ scoria &
lithic AF layers

- 1.0 -Massive scoria & lithic lapilli AF; MS= 1 cm, ML= 1 cm. **ANTI-12**
- .20 -Scoria, pumice & lithic lapilli AF. MS= 1 cm. **ANTI-10**
- .08 -Pumice & lithic AF layer bordered by upper and lower clay seams. **ANTI-9**
- .20 -Lithic, scoria & pumice lapilli AF. MS= 1 cm. Poorly sorted. **ANTI-8**
- .20 -Clay varves; fine laminations
- 1.0 -Black scoracious, med. sandy ash. Coarser lapilli in center, RW near base. **ANTI-5**
- .50 -Clay varves; orange-colored
  -Black coarse sandy lithic AF; RW w/ wavey clay varves. **ANTI-4**
  -Clay varves; orange-colored
- .70 - Black fine scoriaceous ash; RW **ANTI-3**
- .25 -Black med. sandy glass-rich AF; clay seam at base **ANTI-2**
  -Clay varves
- .60 -Coarse scoriaceous sandy AF w/ tabular lithics. w/ interbedded clay seams. **ANTI-1**
- .16 -Debris flow deposit with tabular lava clasts. Stone line related to LGM solufluction?
- 1.6 -Finely stratified & indurated lacustrine unit w/ 1-2 mm thick clay varves & intercalated ash layers
  -Base. Note: Layers **ANTI-6, 7, 11, 13, 15 &16**, of thin sandy scoria AF layers are not shown.
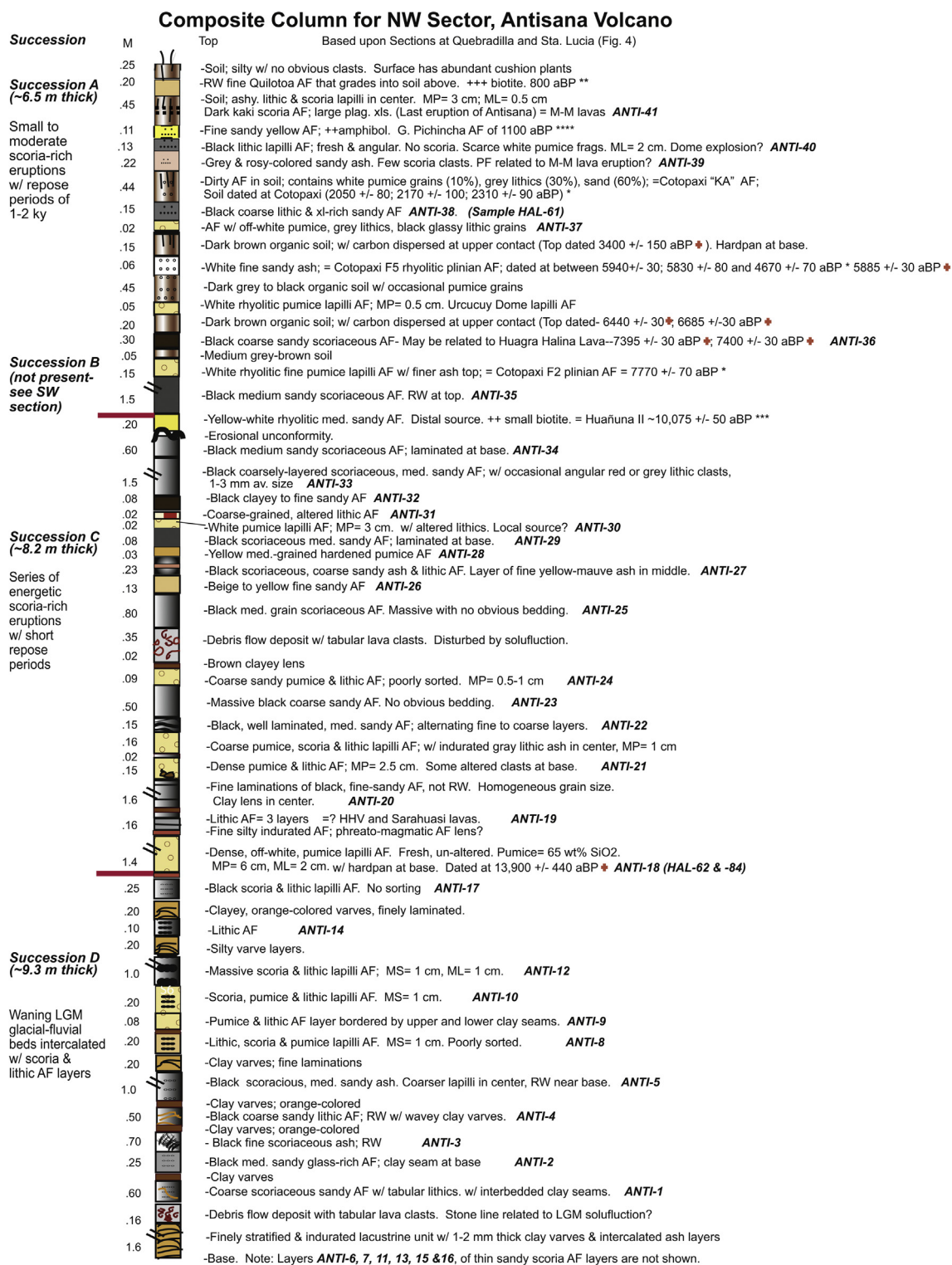
Fig. 9. Composite stratigraphic column for Antisana III's northwest sector.

In general the displayed successions in these columns are comprised of a variable series of dark andesitic scoria and lithic lapilli and ash layers, occasional pumice tephra beds, lava flow units, and to a lesser degree lahar and glacial-fluvial units (Fig. 11). Pyroclastic flow deposits, comprised of small angular clasts of scoria and black lithics in a rosy-colored sandy to gravelly matrix, occur infrequently in the sequences. White to tan-colored distal ash beds as well as gray glacial-fluvial deposits and/or green to maroon-tinted varve layers serve as useful guide units in some successions.

Antisana's youngest lava flows are included in the columns in their respective order. They are all black glassy andesites and dacites and occur only on the lower SW, W, NW, and N flanks of the edifice (Figs. 4 and 6). They vented from the summit cone and many
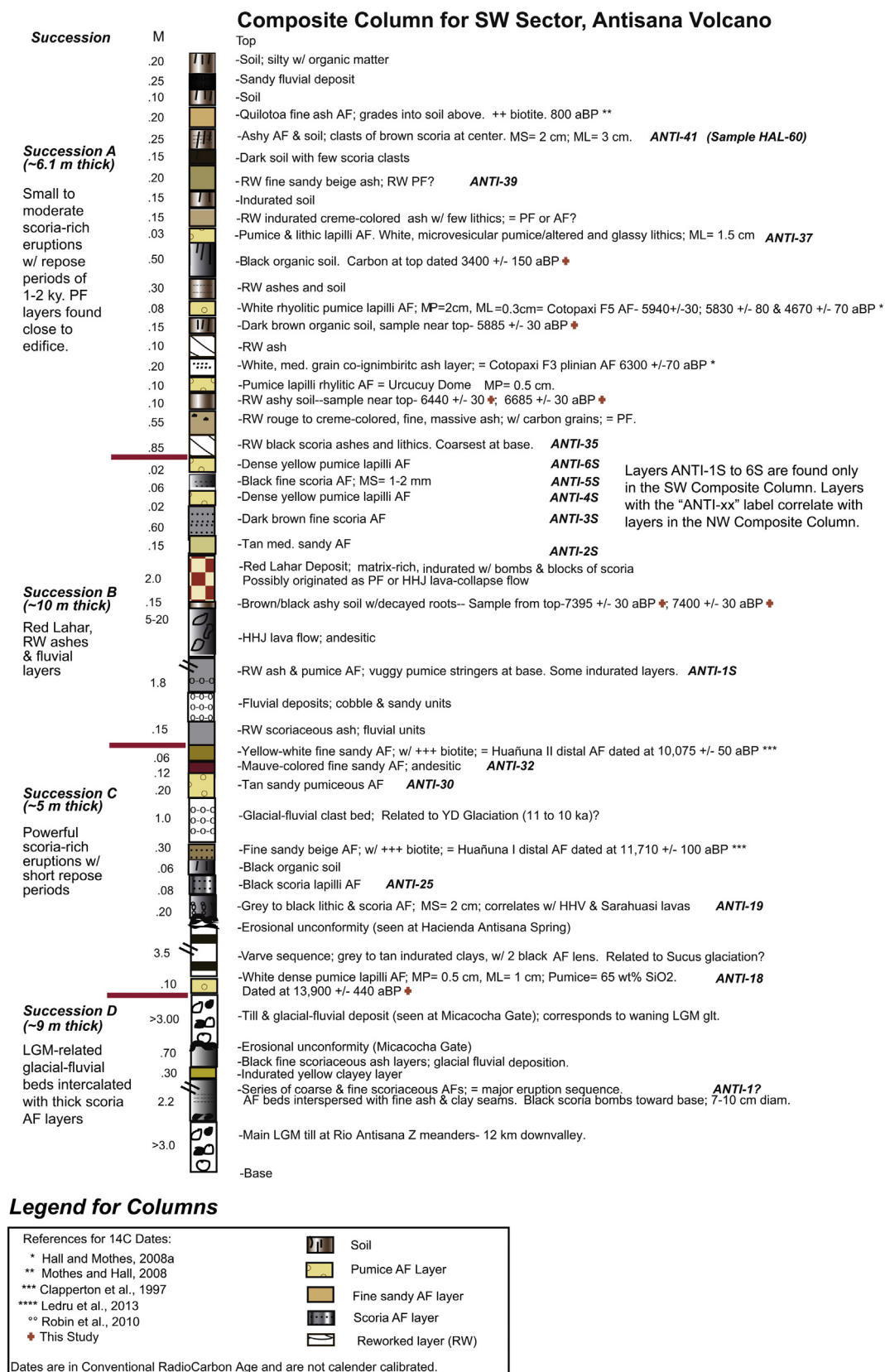
Composite Column for SW Sector, Antisana Volcano

Succession	M		
		Top	

Succession A (~6.1 m thick)

Small to moderate scoria-rich eruptions w/ repose periods of 1-2 ky. PF layers found close to edifice.

- .20 — -Soil; silty w/ organic matter
- .25 — -Sandy fluvial deposit
- .10 — -Soil
- .20 — -Quilotoa fine ash AF; grades into soil above. ++ biotite. 800 aBP **
- .25 — -Ashy AF & soil; clasts of brown scoria at center. MS= 2 cm; ML= 3 cm.   *ANTI-41 (Sample HAL-60)*
- .15 — -Dark soil with few scoria clasts
- .20 — -RW fine sandy beige ash; RW PF?   *ANTI-39*
- .15 — -Indurated soil
- .15 — -RW indurated creme-colored ash w/ few lithics; = PF or AF?
- .03 — -Pumice & lithic lapilli AF. White, microvesicular pumice/altered and glassy lithics; ML= 1.5 cm   *ANTI-37*
- .50 — -Black organic soil. Carbon at top dated 3400 +/- 150 aBP ✚
- .30 — -RW ashes and soil
- .08 — -White rhyolitic pumice lapilli AF; MP=2cm, ML =0.3cm= Cotopaxi F5 AF- 5940+/-30; 5830 +/- 80 & 4670 +/- 70 aBP *
- .15 — -Dark brown organic soil, sample near top- 5885 +/- 30 aBP ✚
- .10 — -RW ash
- .20 — -White, med. grain co-ignimbiritc ash layer; = Cotopaxi F3 plinian AF 6300 +/-70 aBP *
- .10 — -Pumice lapilli rhylitic AF = Urcucuy Dome   MP= 0.5 cm.
- .10 — -RW ashy soil--sample near top- 6440 +/- 30 ✚; 6685 +/- 30 aBP ✚
- .55 — -RW rouge to creme-colored, fine, massive ash; w/ carbon grains; = PF.
- .85 — -RW black scoria ashes and lithics. Coarsest at base.   *ANTI-35*
- .02 — -Dense yellow pumice lapilli AF   *ANTI-6S*
- .06 — -Black fine scoria AF; MS= 1-2 mm   *ANTI-5S*
- .02 — -Dense yellow pumice lapilli AF   *ANTI-4S*
- .60 — -Dark brown fine scoria AF   *ANTI-3S*
- .15 — -Tan med. sandy AF   *ANTI-2S*

Layers ANTI-1S to 6S are found only in the SW Composite Column. Layers with the "ANTI-xx" label correlate with layers in the NW Composite Column.

Succession B (~10 m thick)

Red Lahar, RW ashes & fluvial layers

- 2.0 — -Red Lahar Deposit; matrix-rich, indurated w/ bombs & blocks of scoria Possibly originated as PF or HHJ lava-collapse flow
- .15 — -Brown/black ashy soil w/decayed roots-- Sample from top-7395 +/- 30 aBP ✚; 7400 +/- 30 aBP ✚
- 5-20 — -HHJ lava flow; andesitic
- 1.8 — -RW ash & pumice AF; vuggy pumice stringers at base. Some indurated layers. *ANTI-1S*
- — -Fluvial deposits; cobble & sandy units
- .15 — -RW scoriaceous ash; fluvial units

Succession C (~5 m thick)

Powerful scoria-rich eruptions w/ short repose periods

- .06 — -Yellow-white fine sandy AF; w/ +++ biotite; = Huañuna II distal AF dated at 10,075 +/- 50 aBP ***
- .12 — -Mauve-colored fine sandy AF; andesitic   *ANTI-32*
- .20 — -Tan sandy pumiceous AF   *ANTI-30*
- 1.0 — -Glacial-fluvial clast bed; Related to YD Glaciation (11 to 10 ka)?
- .30 — -Fine sandy beige AF; w/ +++ biotite; = Huañuna I distal AF dated at 11,710 +/- 100 aBP ***
- .06 — -Black organic soil
- .08 — -Black scoria lapilli AF   *ANTI-25*
- .20 — -Grey to black lithic & scoria AF; MS= 2 cm; correlates w/ HHV & Sarahuasi lavas   *ANTI-19*
- — -Erosional unconformity (seen at Hacienda Antisana Spring)
- 3.5 — -Varve sequence; grey to tan indurated clays, w/ 2 black AF lens. Related to Sucus glaciation?
- .10 — -White dense pumice lapilli AF; MP= 0.5 cm, ML= 1 cm; Pumice= 65 wt% SiO2.   *ANTI-18* Dated at 13,900 +/- 440 aBP ✚

Succession D (~9 m thick)

LGM-related glacial-fluvial beds intercalated with thick scoria AF layers

- >3.00 — -Till & glacial-fluvial deposit (seen at Micacocha Gate); corresponds to waning LGM glt.
- .70 — -Erosional unconformity (Micacocha Gate)
- .30 — -Black fine scoriaceous ash layers; glacial fluvial deposition.
- — -Indurated yellow clayey layer
- 2.2 — -Series of coarse & fine scoriaceous AFs; = major eruption sequence.   *ANTI-1?* AF beds interspersed with fine ash & clay seams. Black scoria bombs toward base; 7-10 cm diam.
- >3.0 — -Main LGM till at Rio Antisana Z meanders- 12 km downvalley.
- — -Base

Legend for Columns

References for 14C Dates:		
* Hall and Mothes, 2008a		Soil
** Mothes and Hall, 2008		Pumice AF Layer
*** Clapperton et al., 1997		Fine sandy AF layer
**** Ledru et al., 2013		Scoria AF layer
°° Robin et al., 2010		Reworked layer (RW)
✚ This Study		

Dates are in Conventional RadioCarbon Age and are not calender calibrated.

Fig. 10. Composite stratigraphic column for Antisana III's southwest sector.

reached the broad detrital fan at the western foot of the volcano. The lava flows are of the blocky lava type, having craggy surfaces of scoria blocks and lateral levees (Fig. 1). These lavas tend to form discrete lobes, 30 to 50 m-wide, 10 to 30 m-thick, and 1 to 8 km-

Fig. 11. On the extensive Sta. Lucia depositional fan of Antisana's lower northwest flank a thick sequence of scoria lapilli and ash-rich tephras are interbedded with glacial-fluvial sediments and occasionally with lavas. Photo taken at Site 1 – Sta. Lucia on Fig. 4.

long. Most were glaciated by Late Pleistocene, Holocene, and alpine glaciations, which greatly subdued their original morphology. In general these lavas share the same mineralogy as that described for Antisana II.

The chronological order of the lava flows is based upon criteria such as their location and morphology, their chemical character, tephra stratigraphy, radiocarbon dates, and the Late Pleistocene to Holocene glacial limits. Clapperton et al. (1997) reported that it was possible to place the lower elevation limits of the Late Glacial Maximum (LGM) at ~3500–3600 m, both the Sucus and Younger Dryas (YD) glaciations at ~3900–4000 m, and the Neo-glacial glaciations at ~4200–4400 m in the Ecuadorian Andes. These glaciations are thought to have occurred at ~33 to 15 ka, 13.5 to 12.5 ka, 11 to 10 ka, and in the mid-Holocene, respectively.

During the LGM glaciation a contiguous ice cap covered the entire highlands (Clapperton, 1987) and its terminal moraines are found 15–20 km down valley. Such a massive glaciation would have greatly eroded the terrain, as observed on Antisana's older edifices. YD terminal moraines and till are seen at the 3900 m contour on the N side of Micacocha Lake and can be traced further to the NW. Neo-glacial moraines occur above the 4200–4400 m elevations on Antisana's western flanks, where they are associated with early Holocene lava flows. These elevations and the evidence of glacial erosion are also useful criteria for determining age relationships between lava flows. The well-formed, almost pristine-shape of Antisana III's present cone implies that much of its activity postdates these glaciations. Other nearby volcanic centers, such as Sincholagua, were severely eroded by pre-LGM and LGM glaciers which left only rocky ridges and scarps of their previous edifices, comparable to the erosion endured by the Antisana I and II edifices.

5.2. Stratigraphy

A brief summary of the lithology of each of four stratigraphic successions follows, from the youngest (A) to the oldest (D), as displayed in the two stratigraphic columns (Figs. 9 and 10; Table 2).

Ten regional tephra guide units are recognized in these successions: the 800 aBP Quilotoa ash fall bed (Mothes and Hall, 2008) and the Guagua Pichincha 1100 aBP ash fall unit (Robin et al., 2010; Ledru et al., 2013). Cotopaxi volcano was the source of the "KA" pumice lapilli fall bed (~2100 aBP) and 3 biotite-bearing rhyolitic ash layers, dated at ~5700 aBP (unit F-5), at ~5940 aBP (unit F-4), and at ~7770 aBP for unit F-2 (Hall and Mothes, 2008a). Also two distinct rhyolitic ash layers from nearby Huañuna volcano, dated at 11,710 aBP and 10,075 aBP, respectively, serve as guide units for the LGM and YD glaciations (Clapperton et al., 1997). In addition two other rhyolitic pumice lapilli guide units from nearby Urcucuy volcanic dome are dated at 6685 ± 30 and 6450 ± 30 aBP (this study).

Succession A, the youngest, is ~5–7 m thick and begins with the present soil (~20–25 cm thick). Overall, this succession is comprised mainly of ashy soils in its upper layers and primary to reworked blackish scoriaceous tephra fall beds toward the bottom. Ten primary scoria or ash fall units are recognized, most of which are thin beds, 6–15 cm thick, of brownish-black scoria and lithic lapilli beds, suggesting relatively small eruptions. Occasionally beige-colored pumice fall units are observed that are apparently related to the young dacitic Mauca-Machay (M-M) lavas. However, two of the youngest ash fall beds (HAL-61) are andesitic in composition (57% SiO_2), implying that andesitic magmas still remained at depth. A reddish ash-rich pyroclastic flow bed also occurs in this sequence.

Several lava emission cycles occurred in Succession A. The younger M-M lavas consist of a series of associated flows that cover much of the mid-slopes of the NNE to NNW flanks of Antisana III (Fig. 1). These lavas are black glassy micro-porphyritic dacites (65% SiO_2) with ~20 vol% plag, 4–7% cpx, 6–7% opx, in a ~65% matrix of glass and flow-aligned feldspar microlites. The more frequent presence of amphibole, albeit often altered, distinguishes these late M-M lavas. Slightly older M-M lavas belong to a widespread series of thick flows that descended from the summit crater and covered the cone's N flank, reaching the Rio Blanco Chico valley (Fig. 4); others traveled down the W side of the edifice. Dark gray to black

Table 2
Dimensions and approximate ages of Antisana III's youngest lava flows and associated tephra units.

Lava flows at Antisana	Age control	Length (km)	Area (km²)	Thickness	Volume (km³)	SiO (%)
Mauca-Machay (M-M) younger lavas	800 ± 50 to 1100 ± 40 aBP	7.5	8.0	0.04	0.32	65.2
Mauca-Machay (M-M) older lavas		3.5	3.5	0.04	0.14	63.9
	6450 ± 30; 6685 ± 30 aBP Rhyolitic Pumice layers from Urcucuy dome					
Guagra-Hialina younger (HHJ) lava ≈ Red Lahar Unit	~7400 ± 30 aBP	4.0	3.8	0.04	0.15	62.3
Mud Spring Lava - HAL-51		7.5	6.0	0.03	0.18	62.0
	Younger Dryas Glacial Period from 10,075 ± 50–10,800 ± 100 aBP					
Yana Lava	Early Holocene ~10,800 to 11,710 aBP	3.3	0.7	0.03	0.021	58.6
Micacocha Lava HAL-44		8.5	6.8	0.035	0.24	58.5
Micacocha Lava HAL-45		8.5	2.1	0.030	0.06	58.5
Sarahuasi Lava	≥11,710 ± 100 aBP ≤ 13,900 ± 440 aBP	6.7	3.3	0.040	0.13	57.8
Guagra-Hialina older (HHV) Lava		9.5	4.2	0.02	0.08	57.2
Sta. Lucia lavas						
#3 young		4.5	4.5	0.035	0.16	59.0
#2 mid-		6.3	9.5	0.035	0.33	
#1 older		7.0	10.5	0.035	0.37	
Dacite Pumice Lapilli Fall Bed HAL-62	~13.900 ± 440 aBP					64.9

dacites predominate, bearing 30–40 vol% plag phenocrysts plus 3–5% of both cpx and opx with traces of ol and amph. These dacites have compositions slightly less siliceous (64% SiO_2) than the youngest M-M lavas. The scoria tephras of these two groups of young and older M-M lavas lie between the Quilotoa and Guagua Pichincha distal ash layers, indicating that Antisana's last lava emissions occurred between 800 and 1100 aBP (Table 2).

Succession B includes two marker units, the Red Lahar deposit and a coeval lava flow, which lie ~2.2 m below the Urcucuy marker bed. The lahar deposit is generally <3 m thick, poorly sorted, unstratified, and contains red scoriaceous andesitic clasts up to 1.5 m in diameter, although the average clast size is only 5–15 cm. The red sandy matrix makes up ~50 vol% of the deposit. The flow was somewhat viscous as implied by both the incorporation of pods of unconsolidated materials and the deposit's hummocky morphology upon adjacent floodplains. The presence of fresh scoriaceous lava clasts as well as cauliflower-shaped scoria clots of the younger Huagra-Halina (HHJ) lava flow suggest that the Red Lahar deposit was derived from the advancing near-coeval HHJ lava flow which transformed into a lahar along its course, a likely scenario given Antisana's large volume of snow and ice. This lahar deposit is restricted to the Antisana River drainage and is traceable for ≥15 km down river. At 8 km down valley it consists of an 80 cm-thick, rosy khaki-colored, fine to medium sandy deposit, typically overlain by a 2-3 m-thick soil and tephra accumulation. An organic soil at the lahar's base provided two nearly identical ^{14}C dates of 7400 aBP (this study).

The prominent HHJ lava flow is readily visible at the western foot of Antisana III (Fig. 4). It is a silicic andesite (62% SiO_2) that contains small phenocrysts of plag, opx, cpx, and a trace of ol in a glassy matrix. This unglaciated flow impinges upon the older HHV flow, and thus is younger than that flow. A series of scoria and ash fall units as well as ashy soils, probably related to the HHJ eruption, underlie the HHJ lava. Reworked scoria ash beds and fluvial sediments, with few primary tephra units and soils, comprise the remainder of this succession. The dimensions of this and other lava flows are presented in Table 2.

The Mud Spring Lava flow is a light gray silicic andesite (62% SiO_2) that overlies the Micacocha lava flows at the east end of Micacocha Lake (Fig. 4). It is a micro-porphyritic rock with few clear plag laths, plus pxo and a trace of altered amph in a vitreous matrix. Given its similar appearance and chemistry to the HHJ lavas, it is considered to be a related lava.

The age of Succession B is constrained by the overlying 6450 ± 30 and 6685 ± 30 aBP Urcucuy rhyolitic lapilli ash and the underlying Huañuna II ash dated at ~10,075 aBP (Clapperton et al., 1997).

Succession C mainly concerns the deposits of the YD glacial event and consists of small till deposits, glacial-fluvial beds, fluvial deposits, and interbedded tephra units. The best outcrop of the YD till is found near the Micacocha control gate (3900 m elevation). YD till deposits in this region are overlain by the Huañuna II ash layer (10,075 aBP), while the beginning of the YD glaciation had been placed at ~10,800 aBP (Clapperton et al., 1997). Often associated with these glacial beds are finely-laminated greenish-gray varve deposits and Fe-rich hardpan layers, as well as oxidized scoria lapilli layers.

The pre-YD succession is notable for its lava flows of andesitic composition. The pristine-appearing Yana lava flow (58% SiO_2), which although chemically different than the M-M lavas, appears to be young, unglaciated, and only overlain by thin tephra layers. Other andesitic flows include those of the Micacocha lavas which form two parallel flows and have their termini ~100 m upslope of the present eastern edge of Micacocha lake. There, the terminus of one flow is thoroughly shattered, suggesting that it was quenched upon entering the lake. These two flows are twin coeval flows, being identical gray to black andesites (58% SiO_2) with few micro-phenocrysts of plag, cpx, opx, and ± ol. Their matrices comprise ≤92 vol% of the rock, are mainly glassy, slightly devitrified, and contain feldspar microlites. These flows also predate the YD glacial event and may be slightly younger than the HHV and Sarahuasi lavas.

An underlying pre-YD tephra sequence, ~200 cm thick, consists of at least six black scoria ash and lapilli fall beds and their re-worked equivalents which dominate the sequence in the NW stratigraphic column. These tephra units appear to be related to two glaciated lava flows, the Sarahuasi flow and the older 10 km-long Huagra-Halina flow (HHV) that are found at the western foot of Antisana III (Fig. 4). These are andesitic lavas that share a similar mineralogy (plag, cpx, opx, and ≤5% ol) and chemistry (57–58% SiO_2). They mark a change to an andesitic magmatism, similar but not identical to that of Antisana II. These flows predate the YD glaciation and the Huañuna I ash, but postdate a ~13.9 ka dacitic pumice fall (this study).

A series of older sheet-like lava flows, herein called the Santa Lucia flows, descended the lower NNW flank of Antisana III and followed the Santa Lucia stream valley for several kilometers. This series postdates the 13.9 ka dacitic pumice fall but predates the Huañuna I ash (11.7 ka). They are dark gray slightly porphyritic andesites (59% SiO_2) with small phenocrysts of clear plagioclase

and green olivine in a 90 vol% vitreous matrix (Table 2).

Toward the bottom of Succession C on the lower SW and W flanks of Antisana, reworked ash beds together with varve layers are more than 3 m thick. The probable glacial origin of the varve beds suggests that they may be related to the small Sucus glaciation (~13.5—12.5 ka) observed in Peru (Clapperton et al., 1997). In addition nine scoriaceous ash fall layers are recognized in the NW sector, where they are interbedded with six beds of beige to cream-colored pumiceous ash. As a consequence this succession is notable for the increase in the number and thickness of primary scoria-lithic lapilli beds which suggests an increase in the number of powerful eruptive events with short repose intervals. As observed in Fig. 9, a minimum of 21 eruptions are registered in the 8 m-thick sequence belonging to the ~4000 year andesitic interval between the basal dacitic pumice bed described below and the Huañuna II ash, emphasizing the intense eruptive activity of this period. Clearly the Santa Lucia to Yana sequence corresponds to an andesitic period that existed from at least 14 ka to 10 ka.

The base of this succession is placed at a 1.4 m-thick coarse pumice lapilli fall unit that rests upon a ~13,900 ± 440 aBP peat layer formed on a regional LGM moraine. Clasts of this beige-colored micro-vesicular dacitic pumice range up to 6 cm in size, in addition to the light gray lithic clasts that are $\leq$2 cm in size. The chemistry of this amph-bearing pumice (65% SiO_2) is similar to that of the younger M-M lavas. The fewer varve and glacial-fluvial layers found in this succession, as compared to the underlying sequence, implies waning LGM activity.

Succession D provides evidence of eruptive activity that is best observed at the lower NW foot of Antisana. It consists of ~8 m of scoria and scoria-lithic lapilli fall deposits, each 10—100 cm thick, of both air fall and reworked origin. They are comprised of black, brownish-black, or dark gray scoria and lithic lapilli, however scoriaceous sandy ash layers containing variable amounts of small black lithic clasts are also prevalent. Invariably these are inter-bedded with orange-colored or light gray to tan-colored clayey and silt-rich lamina (varves), thought to represent late LGM glacial outwash. Erosional unconformities and evidence of fluvial re-working are often present.

At the base of Succession D in the SW sector, a 2.2 m-thick sequence of multiple scoria tephra layers overlies a black scoria bomb fall bed (Fig. 10), which lies in turn upon a LGM tillite. This bed is comprised of bombs up to 10 cm in diameter, values which far exceed the bombs of other studied units in Antisana's Late Pleistocene-Holocene stratigraphy, making it one of the most explosive events of this period. Succession D occupies the time interval between the retreat of the LGM glacier (~15 kaBP) and the 13.9 ka pumice fall unit.

5.3. Summary of Antisana III activity

Lava and tephra-producing eruptions dominated the last ~15 ka of Antisana activity, consisting of $\geq$50 eruptions of small to inter-mediate intensity of both andesitic and dacitic compositions. The last lava emission happened between 1100 and 800 aBP and the last important ash-generating eruptions occurred before 800 aBP. Evidence of eruptive activity prior to and during the LGM glaciations is lacking, undoubtedly erased by LGM glaciations or buried by their deposits. Few pyroclastic flow deposits are observed in the studied sections of the west flank, suggesting that very few ever formed, or have not reached the volcano's lower flanks, or were transformed into lahar deposits. Debris flows were generated by volcanic eruptions but also by the melting of the glacier cap, as well as by glacial and morainal lake breakouts; their deposits are mainly observed in stream cuts on the western fan and as far as 15 km down the Antisana River valley.

Marked changes in magma composition distinguish this late phase of activity. The 13.9 ka pumice lapilli fall layer has a dacitic composition (65% SiO_2) comparable to younger M-M lavas. Late Pleistocene tephras and lavas have andesitic tendencies (57—59% SiO_2), notably between 13.9 ka and 10.8 ka. Their compositions are quite similar to late Antisana II andesites (cf. ANT 38 vs. Yana lava — G-157-483). However, by 7.4 ka lava compositions had gradually changed to silicic andesites (62% SiO_2) and then to dacites (63% and later to 65% SiO_2), especially during the late M-M lava stages. The most dacitic compositions appear suddenly at the end of Antisana II and again during late M-M eruptions. The near-contemporaneous emission of both andesite and evolved dacite lavas during Anti-sana III times strongly implies the co-existence of two active magma sources, one probably a remnant of Antisana II andesite activity, the other a new more differentiated Antisana source.

Total volume of lava flows is estimated at 2.2 km^3 for the last ~15,000 years, which represents a minimum rate of production since not all flows were mapped or sampled due to inaccessibility or being covered by moraines and/or later lavas. The dacitic tephra fall of 13.9 ka had the greatest aerial distribution of all young tephra products recognized on Antisana, and its products are found as far as 15 km to the north.

Antisana III appears to be a very young volcano, given the apparent young age of the collapse caldera event, given its small cone (0.6 km^3) built upon the older Antisana II massif, and given the recent and rapid transition to dacitic compositions.

6. Petrography and geochemistry of Antisana Volcano

6.1. Summary of petrographic characteristics

As a whole, Antisana rocks typically have phenocryst contents of 30—50 vol%, always carrying plagioclase (plag), clinopyroxene (cpx), orthopyroxene (opx), magnetite $\pm$ ilmenite (Fe-Ti oxides), and rarely olivine (ol) and amphibole (amph) as accessory minerals. Distinct groupings of plagioclase are recognized in all Antisana lavas, which help to characterize the various magma series. The 1st grouping of plagioclase often occurs as larger (1.2—5.2 mm), resorbed, melt inclusion-rich phenocrysts. The 2nd group is often comprised of intermediate-sized (1.6—2.6 mm) euhedral pheno-crysts, with few inclusions and frequent oscillatory zoning. The 3rd group refers to plagioclase microlites ($\leq$0.1 mm) that may be accompanied by pyroxene microlites in the glass-rich groundmass that generally dominates the rock. Phenocryst sizes vary from 0.6 to 3.0 mm for cpx, $\leq$1.0 mm for opx, and 0.4—0.6 mm for ol.

The andesites of Antisana I have phenocryst contents of 30—45%. Euhedral plagioclase of the 2nd group is very abundant ($\leq$30%) but without notable oscillatory zoning; plagioclase is also present as microlites. 1st group plagioclase is often absent. Both cpx and opx phenocrysts are present in near-equal amounts, totaling 10—15%, but small anhedral crystals of pyroxene also abound in the groundmass. Diamond-shaped olivine may be present but not abundant ($\leq$2%). Minor amounts of Fe-Ti oxides are always present. The glassy matrix, amounting to 55—70%, contains appreciable amounts of plagioclase, pyroxene, and oxides as microlites.

Antisana II lavas are typically two-pyroxene andesites with ~30% of phenocrysts of the 1st and 2nd plagioclase groups. In some cases these lavas lack the 1st groupings of larger, resorbed plagioclase or the 3rd group of plagioclase microlites. The 2nd group of plagioclase is represented by medium-sized euhedral crystals with or without oscillatory zoning. Both opx and cpx are present in approximately equal amounts that total 13—15% of the phenocrysts. The ground-mass amounts to 50—55% and generally carries microlites of plag, cpx, Fe-Ti oxides with interstitial partly devitrified glass.

Antisana III lavas generally carry the same mineralogy as that of

the Antisana I and II lavas, however the 1st plagioclase grouping is uncommon.

6.2. Geochemistry

The succession of Antisana's three edifices recognized in this study allows us to comment on Antisana's chemical evolution. Chemical analyses were published in Bourdon et al. (2002) and new major and trace element analyses are also included in the Appendix, together they comprise 82 whole-rock analyses.

Antisana rocks display a high-K calc-alkaline trend ranging from 53 to 67 wt% SiO_2. Antisana I rocks are mostly basic andesites (53–59% SiO_2) that define a different trend when compared with Antisana II and III samples (Fig. 12). In fact, at similar silica contents, Antisana I samples show lower concentrations in MgO (and some transition elements such as Ni and Cr) and enrichment in Al_2O_3 (and some incompatible elements such as Ba). In contrast, the lavas of the subsequent Antisana II and III edifices share an overlapping trend with gradually increasing silica contents with time (57–67% SiO_2). In fact Antisana III lava flows are characterized by homogeneous dacitic compositions (65–66% SiO_2) that rank among the more differentiated magmas erupted by this volcano. Lastly, the Cuyuja lavas merit special treatment due to their different chemical signature. Although they are roughly contemporaneous with late Antisana II rocks, Cuyuja lavas show an important enrichment in K_2O and in other incompatible trace elements such as Rb, Sr, Ba, La, and Th. Similar compositions have been described in other volcanic systems of the Ecuadorian Eastern Cordillera, namely the Yuyos lava flows of the Chacana volcanic complex (Chiaradia et al., 2014) or the Cono de La Virgen lava flows of Cayambe volcano (Samaniego et al., 2005).

The proximity of Antisana within the greater Chacana complex might lead us to expect some chemical inter-relationships of these two volcanic systems with time. In Fig. 12 the overall field of Chacana volcanic products is drawn together with the individual Antisana samples. Two divergent trends for most incompatible elements (i.e. K_2O, Rb, Th, La) are observed, showing higher values for differentiated samples of Antisana. In addition, Chacana has a greater diversity of calc-alkaline rock types (from andesites to rhyolites) through its 3 + Ma history, as well as with its coeval life with the younger Antisana system. If we compare these two magmatic systems over the same ~400 ka period, Chacana shows a variable spread of rock chemistry over its 56–77% SiO_2 range, while Antisana shows a more steady, gradual enrichment in SiO_2, K_2O, and other incompatible elements with time. It is interesting to note that nearby XVIII century lava flows (shown in Fig. 4) fall in the Chacana field, which strongly argues against a link between these historic lava flows and Antisana volcano. No where nor in any instance are chemically-similar rocks erupted coevally from these two neighboring systems.

In general the major oxides (excepting K_2O and Na_2O, in Fig. 12) show a negative correlation with increasing silica. Light Ion Lithophile Elements (LILE, e.g. Rb, Ba, Th), Light Rare Earth Elements (LREE, e.g. La, Ce), and some High Field Strength Elements (HFSE, e.g. Nb) show broad positive correlations. In contrast, Sr and the transition elements (e.g. Cr, Ni, V) are inversely correlated with silica. Lastly, Y and Heavy Rare Earth Elements (HREE, e.g. Dy, Yb) display scattered trends with almost no variation with silica increase. These chemical trends are easily explained by fractional crystallization processes of a cumulate comprised of the observed minerals (plagioclase, pyroxenes and some olivine and amphibole). Based on these data, together with Sr-Nd isotopic data, Bourdon et al. (2002) interpreted the overall geochemical variation of Antisana as the result of assimilation-fractional crystallization processes that have occurred during magma transfer and storage in

the +50-km-thick Northern Andean crust (Garrison and Davidson, 2003; Bryant et al., 2006; Hidalgo et al., 2012; Barragan et al., 1998). Other processes might also play an important role in magma genesis. For instance, the role of magma mixing in Ecuadorian magmas have been stressed by Schiano et al. (2010), who studied trace element behavior during differentiation and concluded that magma mixing between primitive and differentiated magmas represents a first-order process in arc magma genesis.

Bourdon et al. (2002) also discussed the adakitic signature of some Antisana samples (marked by a strong depletion in Y and HREE). These authors proposed that such a signature results from a heterogeneous, variably-enriched mantle source, metasomatized by hydrous fluids and melts derived from the subducted slab (Bourdon et al., 2002; Samaniego et al., 2005; Hidalgo et al., 2012). However, other models have been proposed that include deep crustal processes that involve melting and/or assimilation of the thick Ecuadorian crust (Garrison and Davidson, 2003; Bryant et al., 2006; Chiaradia et al., 2014). The interested reader should refer to these studies for further details about the proposed petrogenetic models.

In summary, Antisana samples define a monotonous andesitic-dacitic magmatic series with little change throughout its 400 ka lifespan. This behavior contrasts with those of other large long-lasting magmatic systems such as at Cayambe (Samaniego et al., 2005), Mojanda-Fuya Fuya (Robin et al., 2009) or Pichincha (Samaniego et al., 2010) that display notable temporal variations of magma chemistry. In addition, despite its location in the Eastern Cordillera, close to rhyolitic volcanic centers such as at Chacana or Cotopaxi, Antisana rocks do not show a bimodal andesitic-rhyolitic behavior as is the case for the Cotopaxi (Hall and Mothes, 2008a) or Chacana systems (Hall and Mothes, 2008b).

7. Conclusions

The Northern Volcanic Zone of the Andes encompasses the volcanoes of Ecuador and Colombia. This study of Antisana volcano represents the first modern geological and volcanological investigation of Antisana since the late 1890s; it also summarizes its present geochemical understanding and genesis. While many NVZ volcanic centers have been studied to some degree, none has been shown to be the most characteristic of this zone. Here, Antisana is submitted as a good candidate for this distinction. The volcano's development includes the formation and destruction of two older edifices (Antisana I and II) during a 400 + ka period, that witnessed changes from basic andesites to common andesites to Si-rich andesites, and finally during the late Pleistocene to dacites (Antisana III).

Antisana I corresponds to a small highly eroded cone of more basic andesitic composition that suffered limited hydrothermal alteration. Antisana II developed contemporaneously in Antisana I's late stages, and continued, forming the largest volcanic edifice by ≥378 ka, but suffered a sector collapse on its NE side, possibly as late as ~15 ka ago. Subsequently Antisana III's small cone developed on Antisana II's west flank and generated ≥50 eruptions of small to intermediate intensity, of both andesitic and dacitic compositions, during its last 15,000 years. Much of Antisana III's development is well-recorded in its stratigraphy, comprised mainly of interbedded tephra and lavas with late Pleistocene and Holocene glacial deposits.

The three Antisana edifices record more than ~400 ka of magmatic history. The whole rock chemistry of Antisana I is composed of basic andesites (53–58% SiO_2), the rocks of Antisana II are intermediate to Si-rich andesites (58–62% SiO_2), and Antisana III's lavas are comprised chiefly of dacites (63–66% SiO_2). During its long history there were no major changes in its phenocryst
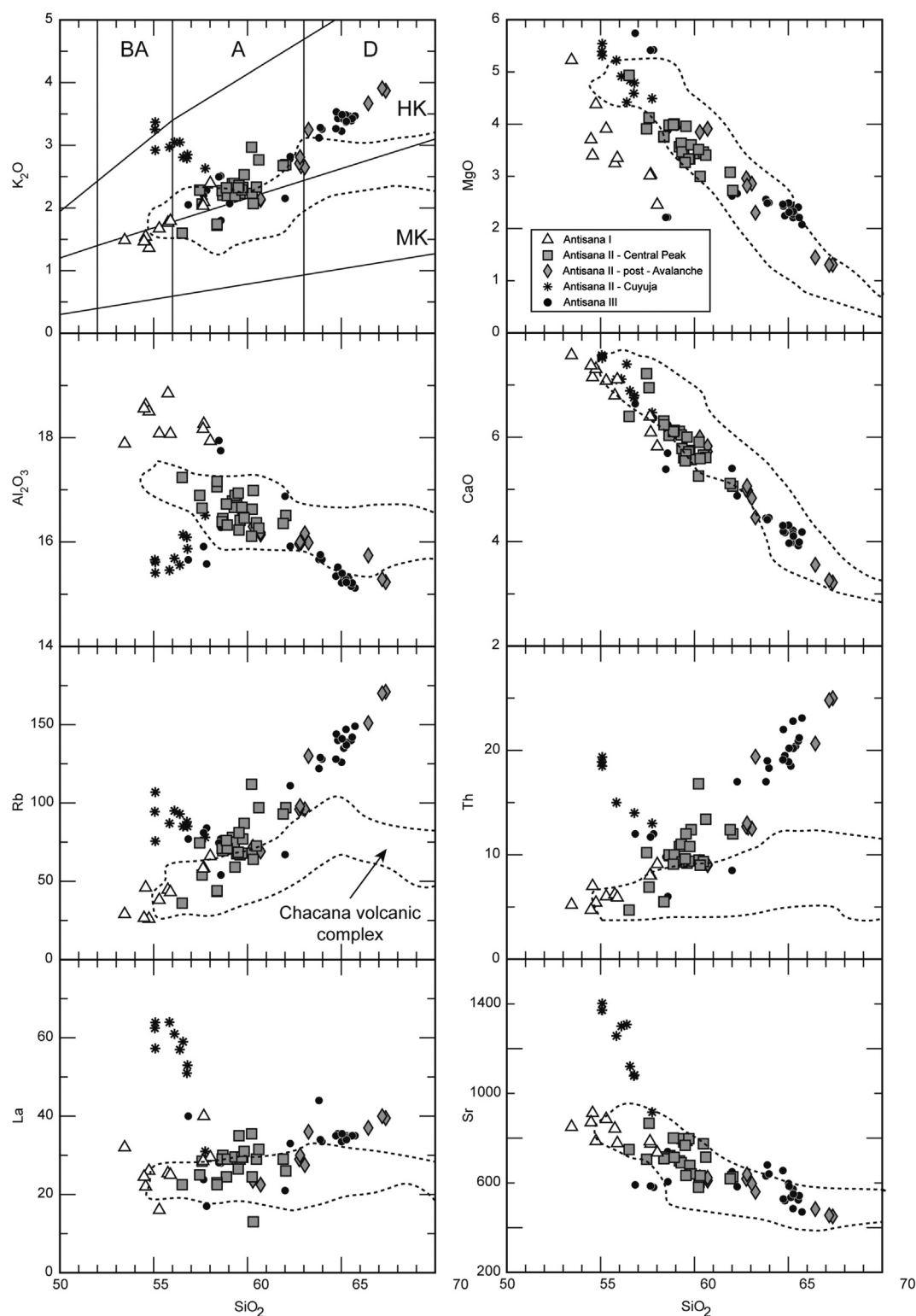
Fig. 12. Selected major oxides and minor elements plotted against silica. SiO vs. K_2O classification diagram modified from Peccerillo and Taylor (1976). BA = basic andesites, A = andesites, D = dacites, MK = medium K_2O levels, HK = high K_2O levels. Note that Antisana I, II, and III have similar differentiation trends, the exception being MgO and Ba plots of Antisana I with separate, but parallel trends. Also note that the Cuyuja samples have distinct groupings, not akin to the Antisana samples. Analyses taken from Bourdon et al. (2002) and the Appendix of this study.

mineralogy that consisted of plagioclase, both clino- and ortho-pyroxene, plus Fe-Ti oxides and occasional traces of olivine and amphibole, despite the magma's progressive chemical change from basic andesites to silicic dacites. Antisana's two neighboring strato-

volcanoes, Cotopaxi and Cayambe, have had, however, complex petrologic histories due to magma mixing and rhyolitic injections (Hall and Mothes, 2008a; Garrison et al., 2011; Samaniego et al., 2005). In addition, although nestled within the Chacana caldera,

Antisana's magmatic activity shows no close chemical relationship to that of Chacana.

Contrasting with the singular chemical trends of Antisana's main lavas is the short-lived anomalous Cuyuja event whose lava flows (~11 km^3) of homogeneous andesitic lava (56 wt% SiO_2) are chemically unlike that of other Antisana lavas. These lava flows, one more than 73 km long, apparently had their origin on Antisana II's upper flanks about 210 ka ago. The Cuyuja lavas have similarities to the high-Mg andesites of Chacana's Yuyos lavas that contain high contents of incompatible elements (Ba, Sr, Th), as well as compatible elements (Ni, Cr), as reported by Chiaradia et al. (2014). They attributed such characteristics to young subduction-related magma genesis.

Acknowledgements

Appendix A. Supplementary data

Supplementary data related to this article can be found at http://dx.doi.org/10.1016/j.jsames.2016.11.005.

References

Barragan, R., Geist, D., Hall, M., Larson, P., Kurz, M., 1998. Subduction controls on the compositions of lavas from the Ecuadorian Andes. Earth Planet. Sci. Lett. 154, 153–166.

Bourdon, E., Eissen, J.-P., Monzier, M., Robin, C., Martin, H., Cotton, J., Hall, M., 2002. Adakite-like lavas from Antisana Volcano (Ecuador): evidence for slab melt metasomatism beneath the Andean Northern Volcanic Zone. J. Petrol. 43, 199–217.

Bryant, J., Yogodzinski, G., Hall, M., Lewicki, J., Baily, D., 2006. Geochemical constraints on the origin of volcanic rocks from the Andean Northern Volcanic Zone. Ecuad. J. Petrol. 47, 1–29.

Cáceres, B., Maisincho, L., Taupin, J., Bucher, R., Paredes, D., Villacis, M., Chazarin, J., Francou, B., Cadier, E., 2004. Glacier 15 del Antisana (Ecuador). Balance de masa, topografía, meteorología e hidrología. Año 2003. Informe 6. IRD, INAMHI, EMAAP-Quito: 100 pp.

Chiaradia, M., Müntener, O., Beate, B., 2014. Quaternary Sanukitoid-like Andesites generated by intracrustal processes (Chacana caldera complex), Ecuador: implications for Archean Sanukitoids. J. Petrol. 55, 769–802.

Clapperton, C., 1987. Glacial morphology, Quaternary glacial sequence and paleo-climatic inferences in the Ecuadorian Andes. In: International Geomorphology Part II, pp. 843–870.

Clapperton, C., Hall, M., Mothes, P., et al., 1997. A younger Dryas icecap in the equatorial Andes. Quat. Res. 47, 13–28.

Egred, J., 2010. Historia de la Actividad del Volcán Antisana. Instituto Geofísico, Quito, Ecuador.

Garrison, J., Davidson, J., 2003. A dubious case for slab melting in the Northern Volcanic Zone of the South American Andes. Geology 71, 151–154.

Garrison, J., Davidson, J.P., Hall, M.L., Mothes, P.A., 2011. Geochemistry and petrology of the most recent deposits from Cotopaxi Volcano, Northern Volcanic Zone, Ecuador. J. Petrol. 52 (9), 1641–1678.

Hall, M., 1977. El Volcanismo en el Ecuador. Instit Panamerican Geografía Historia, Quito, 120 pp.

Hall, M., Beate, B., 1991. El Volcanismo Plio-Cuaternario en los Andes del Ecuador. In: Mothes, P. (Ed.), El Paisaje Volcánico de la Sierra Ecuatoriana -Estudios de Geografía, vol. 4, pp. 15–18.

Hall, M., Mothes, P., 2008a. The rhyolitic-andesitic eruptive history of Cotopaxi volcano, Ecuador. Bull. Volcanol. 70, 675–702. http://dx.doi.org/10.1007/s00445-007-0161-2.

Hall, M., Mothes, P., 2008b. The Chacana Caldera Complex in Ecuador. IOP Conf Series. http://dx.doi.org/10.1088/1755-1307/3/1/012004.

Hall, M., Beate, B., von Hillebrandt, C., 1989. Mapa de Los Peligros Volcánicos Potenciales Asociados con el Volcán Antisana. Esc. 1:50.000. Instituto Geofísico, Esc. Pol. Nac., Quito.

Hall, M., Samaniego, P., Le Pennec, J.-L., Johnson, J., 2008. Ecuadorian Andes volcanism: a review of Late Pliocene to present activity. J. Volcan. Geotherm. Res. 176, 1–6.

Hastenrath, S., 1981. The Glaciation of the Ecuadorian Andes. Balkema Publishers, Rotterdam, A.A, 159 pp.

Hidalgo, S., Gerbe, M., Martin, H., Samaniego, P., Bourdon, E., 2012. Role of crustal and slab components in the Northern Volcanic Zone of the Andes (Ecuador) constrained by Sr-Nd-O isotopes. Lithos 132–133, 180–192.

Humboldt, A., 1837-38. Geognostische und physikalische beobachtungen uber die vulkane des hochlandes von Quito. Poggend. Ann. Phys. Chem. 193–219. Bd 40: 161-93; Bd 44.

Keszthelyi, L., Self, S., 1998. Some physical requirements for the emplacement of long basaltic lava flows. J. Geophys. Res. 103, 27,447–27,463.

Ledru, M.-P., Jomelli, V., Samaniego, P., Vuille, M., Hidalgo, S., Herrera, M., Ceron, C., 2013. The Medieval climate Anomaly and the Little Ice Age in the eastern ecuadorian Andes. Clim. Past 9, 307–321.

Meyer, H., 1907. Den Hochanden von Ecuador (in Spanish). Anal Univ Central LX, LXI, LXII, Quito, p. 522.

Monzier, M., Robin, C., Samaniego, P., Hall, M., Cotten, J., Mothes, P., Arnaud, N., 1999. Sangay volcano, Ecuador: structural development, present activity and petrology. J. Volcan. Geotherm. Res. 90, 49–79.

Mothes, P., Hall, M., 2008. Rhyolitic calderas and centers clustered within the Active Andesitic belt of Ecuador's eastern Cordillera. IOP Conf. Ser. http://dx.doi.org/10.1088/1755-1307/3/1/012007.

Nocquet, J.M., Villegas-Lanza, J.C., Chlieh, M., Mothes, P., Rolandone, F., Jarrin, P., Cisneros, D., Alvarado, A., Audin, L., Bondoux, F., Martin, X., Font, Y., Régnier, M., Vallée, M., Tran, T., Beauval, C., Maguiña, J.M., Mendoza, W., Martinez, H., Tavera, J., Yepes, H., 2014. Motion of continental slivers and creeping subduction in the northern Andes. Nat. Geosci. 7, 287–291. http://dx.doi.org/10.1038/ngeo2099.

Opdyke, N., Hall, M., Mejia, V., Huang, K., Foster, D., 2006. Time-averaged field at the equater: results from Ecuador. Geochem. Geophys. Geosyst. 7, Q11005. http://dx.doi.org/10.1029/2005GC001221.

Peccerillo, A., Taylor, S., 1976. Geochemistry of Eocene calc-alkaline volcanic rocks from Kastamonu area, northern Turkey. Contrib. Mineral. Petrol. 58, 63–81.

Reiss, W., Stübel, A., 1869-1902. Das Hochgebirge der Republik Ecuador II: Petrographische Untersuchungen (Ostkordillere: Berlin).

Robin, C., Eissen, J.-P., Samaniego, P., Martin, H., Hall, M., Cotton, J., 2009. Evolution of the Late Pleistocene Mojanda-Fuya Fuya volcanic complex (Ecuador), by progressive adakitic involvement in mantle magma sources. Bull. Volcan. 71, 233–258.

Robin, C., Samaniego, P., Le Pennec, J.L., Mothes, P., van der Plicht, J., 2010. New radiometric and petrological constraints on the evolution of the Pichincha volcanic complex (Ecuador). Bull. Volcan. 72 (9), 1109–1129. http://dx.doi.org/10.1007/s00445-010-0389-0. · October 2010.

Samaniego, P., Martin, H., Monzier, M., Robin, C., Fornari, M., Eissen, J.-P., Cotton, J., 2005. Temporal evolution of magmatism at Northern Volcanic Zone of the Andes: the geology and petrology of Cayambe volcanic complex (Ecuador). J. Petrol. 46, 2225–2252.

Samaniego, P., Robin, C., Chazot, G., Bourdon, E., Cotton, J., 2010. Evolving metasomatic agent in the Northern Andean subduction zone, deduced from magma composition of the long-lived Pichincha volcanic complex (Ecuador). Contrib. Mineral. Petrol. http://dx.doi.org/10.1007/s00410-009-0475-5.

Sauer, W., 1965. Geología del Ecuador (Editor, Min. Educación, Quito).

Schiano, P., Monzier, M., Eissen, J.-P., Martin, H., Koga, K., 2010. Simple mixing as the major control of the evolution of volcanic suites in the Ecuadorian Andes. Contrib. Mineral. Petrol. 160, 297–312.

Trenkamp, R., Kellogg, J., Freymueller, J., Mora, H., 2002. Wide plate margin deformation, south Central America and northwestern South America: CASA GPS observations. J. South Am. Earth Sci. 15, 157–171.

Whymper, E., 1987. Travels Amongst the Great Andes of the Equater. Peregrine Smith Books, Salt Lake City, 456 pp.

Wolf, T., 1892. Geografía y Geología del Ecuador. Brockhaus, Leipzig, 671 pp.